Ka-Band Wide-Bandgap Solid-State Power Amplifier: Hardware Validation

L. Epp,[1] P. Khan,[1] and A. Silva[1]

Motivated by recent advances in wide-bandgap (WBG) gallium nitride (GaN) semiconductor technology, there is considerable interest in developing efficient solid-state power amplifiers (SSPAs) as an alternative to the traveling-wave tube amplifier (TWTA) for space applications. This article documents proof-of-concept hardware used to validate power-combining technologies that may enable a 120-W, 40 percent power-added efficiency (PAE) SSPA. Results in previous articles [1–3] indicate that architectures based on at least three power combiner designs are likely to enable the target SSPA. Previous architecture performance analyses and estimates indicate that the proposed architectures can power combine 16 to 32 individual monolithic microwave integrated circuits (MMICs) with >80 percent combining efficiency. This combining efficiency would correspond to MMIC requirements of 5- to 10-W output power and >48 percent PAE. In order to validate the performance estimates of the three proposed architectures, measurements of proof-of-concept hardware are reported here.

I. Introduction

In previous articles, the performance estimates for three solid-state power amplifier (SSPA) architectures were developed [1–3]. Results of targeted hardware validation activities are presented in this article. Given budget and time constraints, validation activities were limited to measuring hardware for two of the three proposed architectures. The next section describes these hardware validation activities. Following this discussion, this article will discuss the performance summaries for the three SSPA architectures and needed follow-on work.

---

[1] Communications Ground Systems Section.

This research was carried out at the Jet Propulsion Laboratory, California Institute of Technology, and was sponsored by Glenn Research Center, and the National Aeronautics and Space Administration. Reference herein to any specific commercial product, process, or service by trade name, trademark, manufacturer or otherwise, does not constitute or imply its endorsement by the United States Government or the Jet Propulsion Laboratory, California Institute of Technology.

II. Hardware Validation

A. Prototype Waveguide Binary Combiner

1. Mechanical Design and Fabrication. A prototype combiner, Fig. 1, was designed, fabricated, and tested to demonstrate the thin-film resistive septum concept [4].[2] As indicated, the input full-height waveguides are matched to reduced-height waveguides using stepped impedance transformers. Mitered E-plane bends are included in the design for convenient layout of ports. An effort was made to maintain accurate symmetry about the y–z plane. The septum itself, for example, was implemented by stacking two 0.13-mm-thick alumina substrates. The mating surface of one substrate was coated with TaN (128 ohms/sq.) resistive sheet. This approach resulted in accurate placement of the resistive sheet on the symmetry plane with equal thickness of dielectric on either side. Standard tolerance (±10 percent) in sheet resistance was found to be adequate for implementing the prototype design.

2. 2-Way Combiner Results. Four prototype units were fabricated and measured. As shown in Fig. 1, the waveguide was machined in two symmetric halves. It is important to note that the blocks were designed to equally split the waveguide along its broad wall. Since no surface current flows across

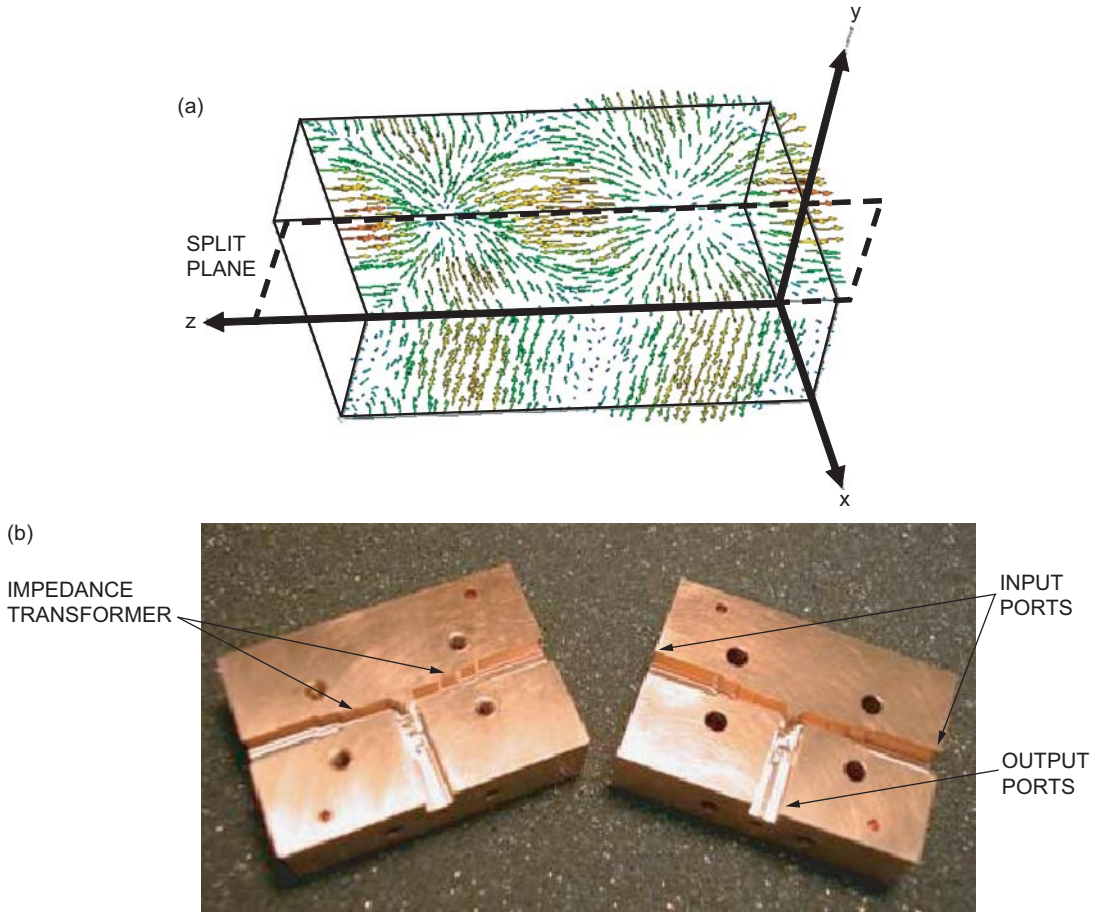

Fig. 1. Disassembled prototype septum combiner: (a) rectangular waveguide surface current for the TE_{10} propagation mode and (b) identical halves of a split-block design.

[2] A. R. Khan, L. W. Epp, D. J. Hoppe, and D. Kelley, *Thin-Film Resistive Septum Waveguide Power Combiner*, JPL New Technology Report no. 40903 (internal document), Jet Propulsion Laboratory, Pasadena, California, November 16, 2004.

the mating surface between the two blocks, i.e., across the $z = a/2$ plane, no additional loss is incurred due to the split-block design. Figure 2 illustrates the measured performance compared to analysis. The agreement is good, and the differences are within the fabrication and assembly tolerances. The four prototype units exhibited little variation in performance. The worst performing unit had an input match >25 dB, output match >31 dB, insertion loss <0.1 dB, and isolation >27 dB over the 31- to 36-GHz band. Among the four prototype units, the worst amplitude balance was 0.065 dB, and the worst phase balance was 0.75 deg. This excellent performance demonstrates the potential for this power combiner technology to enable a new class of high-power, high-efficiency, solid-state amplifiers.

B. Prototype Waveguide Radial Combiner

This section will discuss a prototype $N = 24$ combiner that was designed at 32 GHz (Ka-band) and demonstrated over the band of 31 to 36 GHz with an input match <-20 dB under equal excitation of all input ports, an output match <-24 dB at the rectangular waveguide (RWG) port of the "Marie"

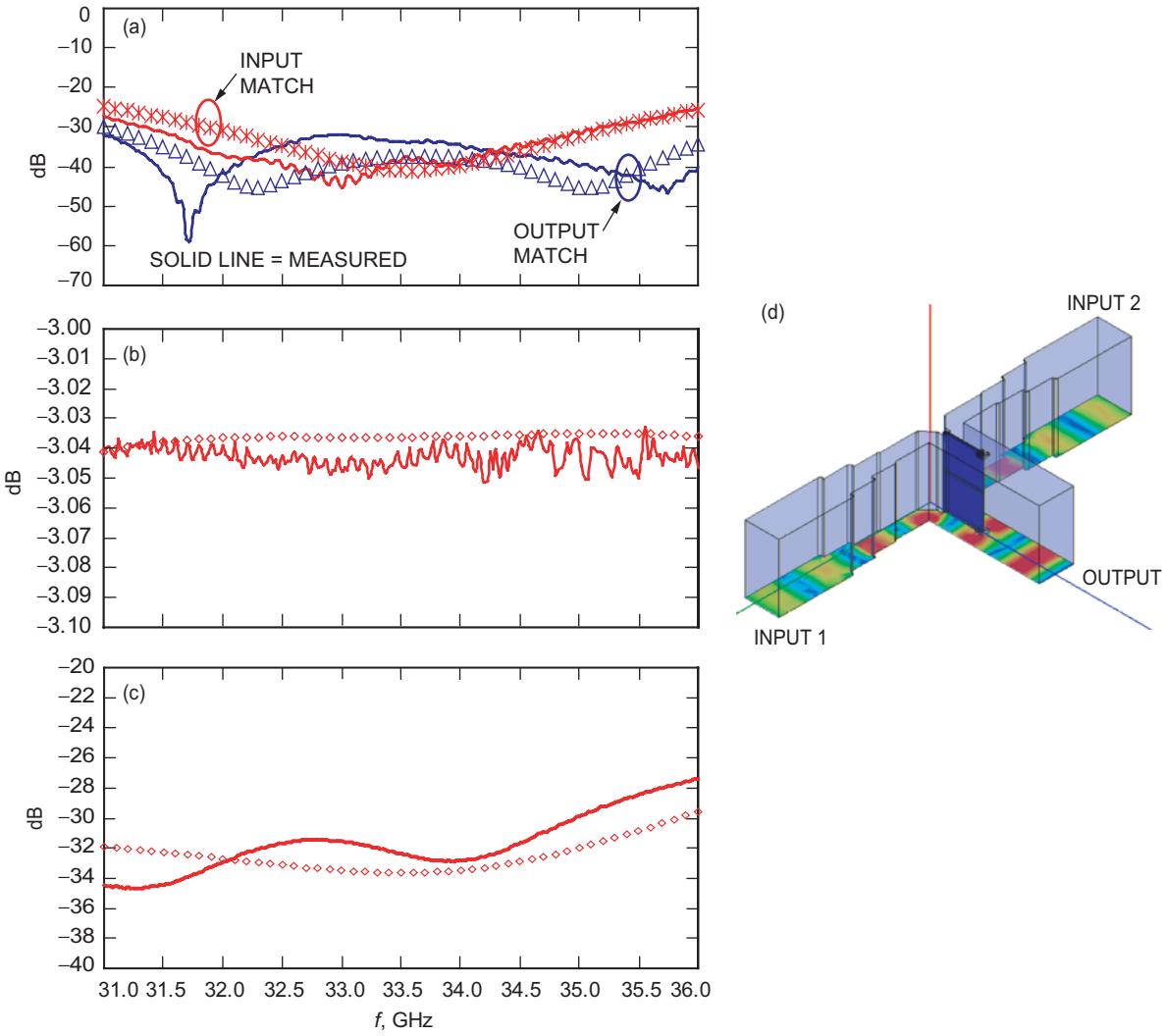

Fig. 2. Analysis and measured results for a 2-way septum combiner: (a) match, (b) coupling, (c) isolation, and (d) geometry.

transducer, and an insertion loss <0.4 dB [5].[3] The functional bandwidth of the combiner exceeds the initial design band requirements of 31 to 36 GHz.

1. Mode Transducer Design and Fabrication. There are several possible solutions for the mode transducer design. The most obvious would be the use of a so-called "flower-petal" transducer [6]; see Fig. 3. There is a limited availability of these parts from at least one commercial vendor [7]. Arguably the main drawback of the flower-petal transducer approach is the bandwidth of ∼6 percent at Ka-band. Even Hoag et al. point out that, when broad bandwidth is required, other approaches are better suited for communications systems [6]. Results for the commercial flower-petal input match are shown in Fig. 4. This shows that the 16-dB bandwidth for this part is 2.4 GHz, which is less than half the required bandwidth.

There are other drawbacks to the flower-petal transducer. Although alternative mode transducers such as the Marie design are often longer in length, the commercial flower-petal insertion loss specifications are as high as 0.3 dB within a voltage standing wave ratio (VSWR) range <1.4 [7] (this translates into an input match of −16 dB). This was verified by measurement (see Fig. 5), which also showed trapped modes in the back-to-back measurement. Due to these limitations, the work here looked at a more broadband mode transducer design based on the work of either Saad et al. [8] or Wolfert [9].

To convert the radial base circular waveguide output back to rectangular waveguide, a mode transducer was designed based on the concept of Saad et al. [8] (see Fig. 6). This part has one plane of symmetry that is not exhibited by the design of Wolfert [9], which makes it more amenable to solution. The mode transducer originally was broken into three sections that were individually designed. Although the mating profiles of the three sections approximate those of Saad et al. [8], there is insufficient information in this previous work to define the contours that connect these profiles, or the profiles themselves for this frequency band. Other factors, such as poor performance below 33 GHz, did not meet the requirements of this task. By properly designing new profiles, contours, and lengths of each section, it was found to be possible to choose a circular waveguide size that would meet the requirements of the radial combiner design by allowing for a sufficiently large circular waveguide to combine 24 inputs that would operate

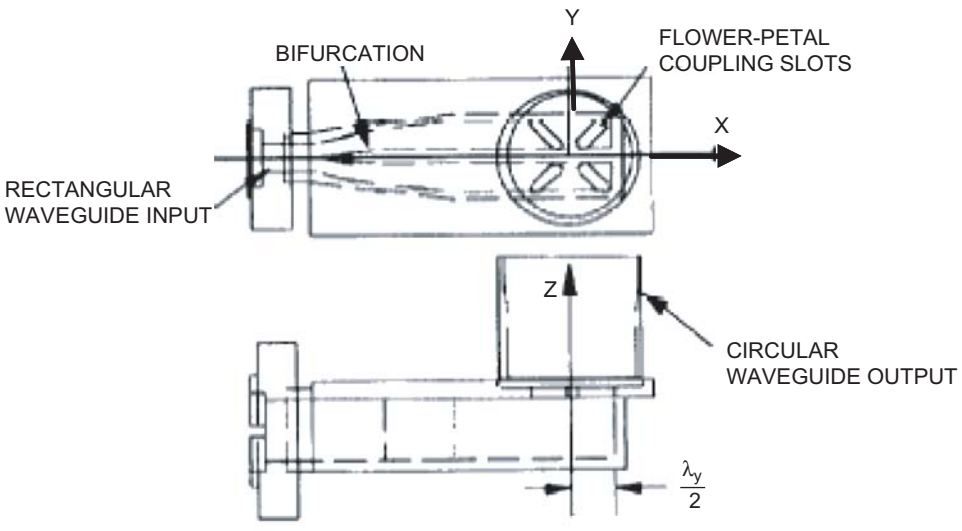

Fig. 3. The flower-petal transducer concept as depicted by Hoag et al. [6].

[3] L. W. Epp, A. R. Khan, D. J. Hoppe, and D. Kelley, *Wideband 24-Way Radial Power Combiner/Divider Fed by a Marie Transducer*, JPL New Technology Report no. 41511 (internal document), Jet Propulsion Laboratory, Pasadena, California, December 7, 2004.

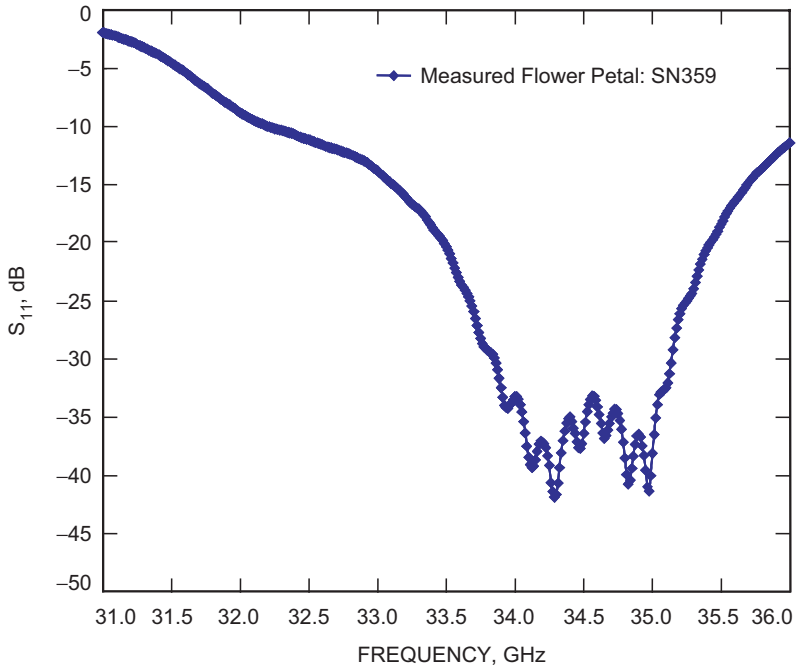

Fig. 4. WR-28 port match of commercial flower-petal mode transducer showing limited bandwidth.

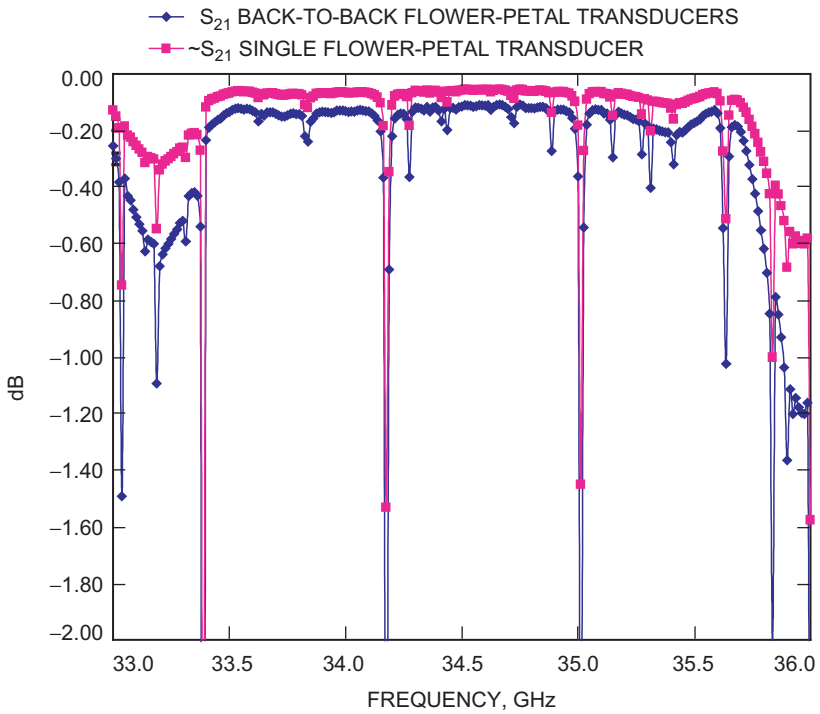

Fig. 5. Measured S_{21} (relates to insertion loss) of two commercial flower-petal transducers (WR-28) back-to-back. The large insertion loss spikes indicate the presence of trapped modes.

Fig. 6. Prototype of the Marie-mode transducer.

from 31 to 36 GHz. It was found that the mode transducer could be designed for two different rectangular waveguide outputs by modification of only section 1, leading to a design for multiple frequency ranges with a common circular waveguide input.

2. Mode Transducer Results. To keep calculation times manageable, the transducer of Fig. 6 first was analyzed in three sections, as originally was done by Saad et al. [8]. By using an E-wall or perfect electric conductor (PEC) boundary along the plane of symmetry of the part (splits the short wall of the rectangular waveguide input of the mode transducer), the entire three-section part was simulated. This allowed a final optimization of the output waveguide size to eliminate unwanted modes, i.e., modes that are not the TE_{01} circular waveguide mode.

The results of the Marie transducer measurements are given in Figs. 7 and 8. The results for the prototype with the WR-28 output are shown in Figs. 7 and 8, which show the match <-30 dB over the bandwidth measure on part no. SN1, and similarly good behavior from part no. SN2. The mode transducer insertion loss can be calculated by measuring the two transducers SN1 and SN2 back-to-back, and dividing the loss by half. The agreement with theory and design in the S_{21} measurements is excellent.

Figure 8 shows a dramatic improvement in the reduction of trapped modes in the broadband Marie transducer, as compared to the narrowband flower-petal transducer response of Fig. 5, in back-to-back measurements. These modes could be caused by slight tolerances in manufacturing between the two Marie transducers and/or indicate the presence of higher-order modes beyond the desired TE_{01} mode. For example, the TM_{11} mode has the same cutoff frequency in circular waveguide as the TE_{01} mode. For a very narrowband application, Fig. 5 shows that the shorter flower-petal design exhibits a smaller insertion loss.

3. Radial Base Design and Fabrication. In order to increase the number of combining ports, referred to here as the order N of the combiner, the full-height waveguides at the combining ports are matched to reduced-height waveguides. This is done by incorporating the stepped-impedance transformers from the septum combiner. This is a novel change from existing radial combiners, since the stepped-impedance transformers allow for reduced-height waveguides inside the radial base, where the height of the waveguides limits the order N of combining. Using this approach, a prototype achieved the power-combining order $N = 24$. A matching post at the bottom of the radial base was able to match the reduced-height rectangular waveguides into the circular waveguide that feeds the mode transducer (see Fig. 9).

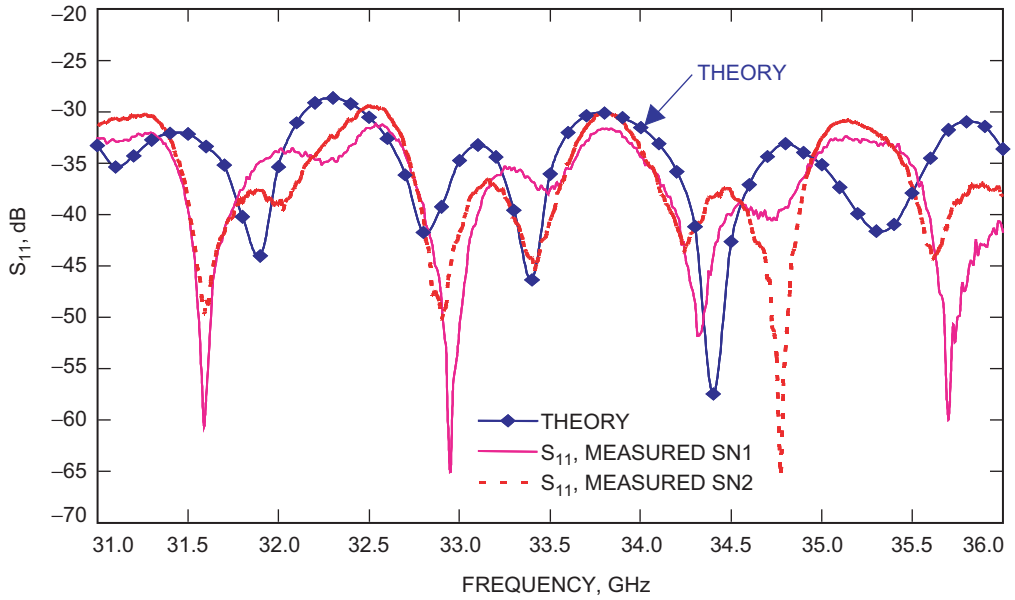

Fig. 7. WR-28 port match of the prototype Marie-mode transducer with a circular waveguide (CWG) load.

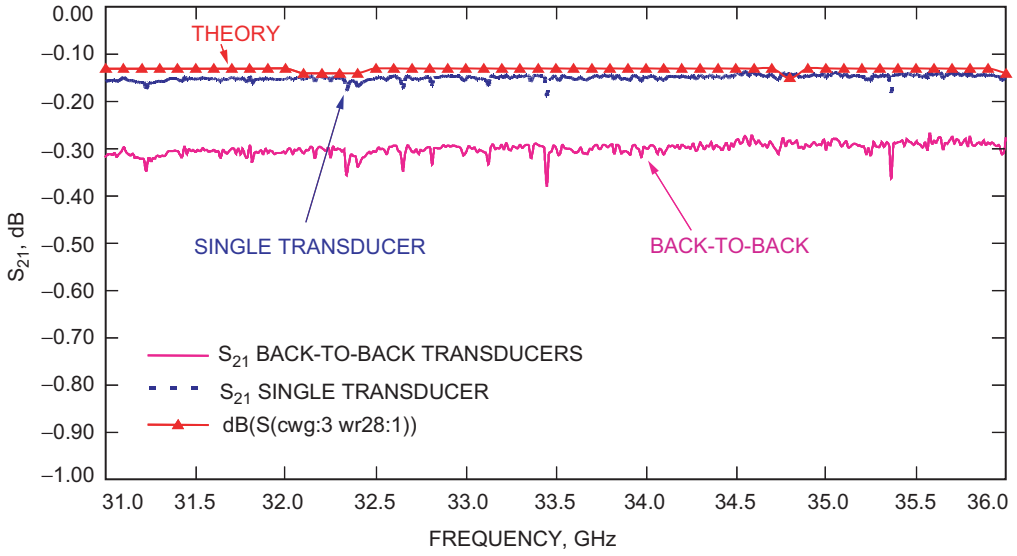

Fig. 8. Measured S_{21} (relates to insertion loss) of the prototype Marie-mode transducer (WR-28).

As described previously, the radial base is combined with the mode transducer to form the prototype $N = 24$ combiner. The basis for choosing this combination was the work of Chen [10], who demonstrated a 19-way power divider. The fundamental differences between the approach of Chen [10] and this work include the frequency change, the impedance transformers, the matching stub of the radial base, higher $N = 24$ combining, and the re-designed mode transducer design. Another fundamental change was the desire not to incorporate resistive cards into the radial base. While a resistive card adds isolation, the asymmetry of the resistive card approach leads to a large 0.72-dB insertion loss [10], a potential power limitation of the device, and a more difficult tolerance issue to avoid additional asymmetry at the higher-frequency design needed. In order to reduce this loss, the current combiner was designed to work without resistive cards in the radial base. Therefore, if isolation is desired, it may be added externally.

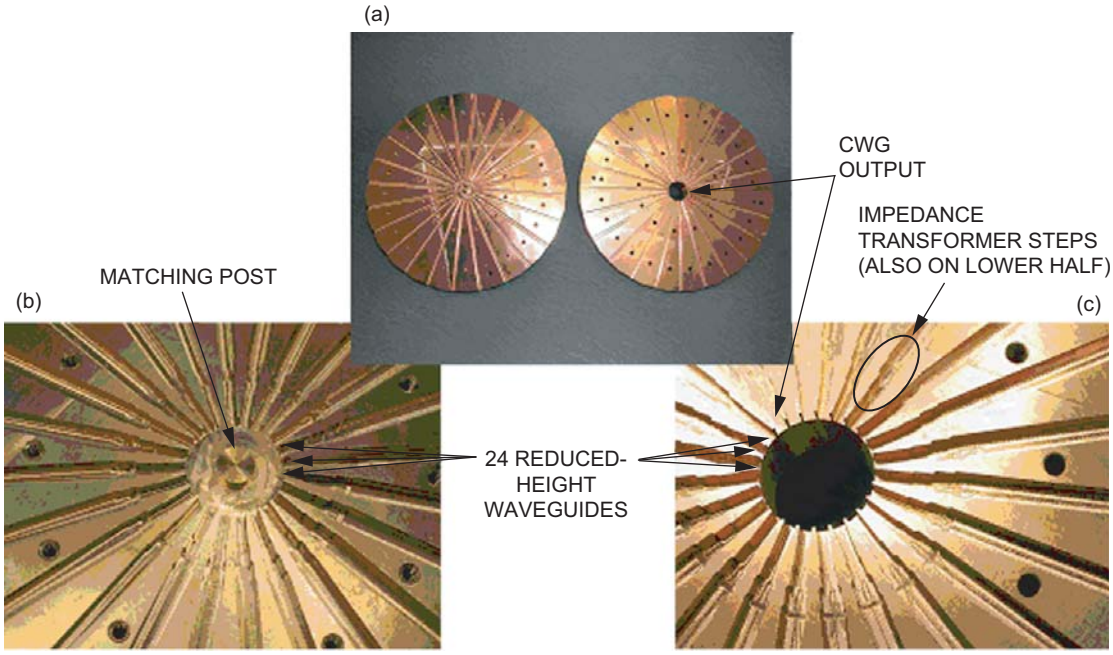

Fig. 9. Prototype of the 24-way radial base showing reduced-height waveguides, impedance transformers, and the matching post: (a) the two halves of the radial base, (b) lower half of the split-block design, and (c) upper half of the split-block design.

As shown in Fig. 9, the radial base prototype was machined in two halves. Note that the blocks were, as in the septum combiner, designed to equally split the waveguide along its broad wall. Since no surface current flows across the mating surface, no additional loss is incurred due to a split-block design.

The measured performance compared to analysis for the radial base without the transducer is shown in Fig. 10. The comparison in Fig. 10 is for equal excitation at all input ports, which can be compared to the commercial simulation and design tool, Ansoft's High Frequency Structure Simulator (HFSS) [11]. For these measurements, the circular waveguide port is a matched (circular) load and symmetry was not assumed. Isolation between the input ports of the radial base is shown in Fig. 11.

4. 24-Way Combiner Results. Figures 12 through 18 illustrate the measured performance compared to analysis for the 24-way power combiner, which consists of the mode transducer connected to the radial base. The output match of the combiner is shown in Fig. 12, which shows a match <-24 dB over the band. Together, the mode transducer and radial base have one plane of symmetry. In an effort to deduce possible manufacturing tolerance effects, the transducer was mounted on the radial base in the two "orthogonal" configurations. The Marie mode transducer has one plane of symmetry. If the radial base is manufactured to tolerance, there are two ways to mount the mode transducer: one with the transducer's symmetry plane between two RWG ports in the base (ports 24 and 1), and one with the transducer's symmetry plane aligned with an RWG input port (port 1).

In Fig. 12, as in all measurements, there is not a significant effect on the output match caused by the orientation of the mode transducer. Therefore, for brevity, the measurements of the other orientation will not be shown. The output match as shown in Fig. 12 can be compared to the radial base output match of Fig. 10 and the mode transducer output match of Fig. 7.

Figure 13 is the measured combiner input match for equal excitation of all input ports, showing a match <-20 db over the band for the waveguide input port 1. Symmetry was not assumed in computing

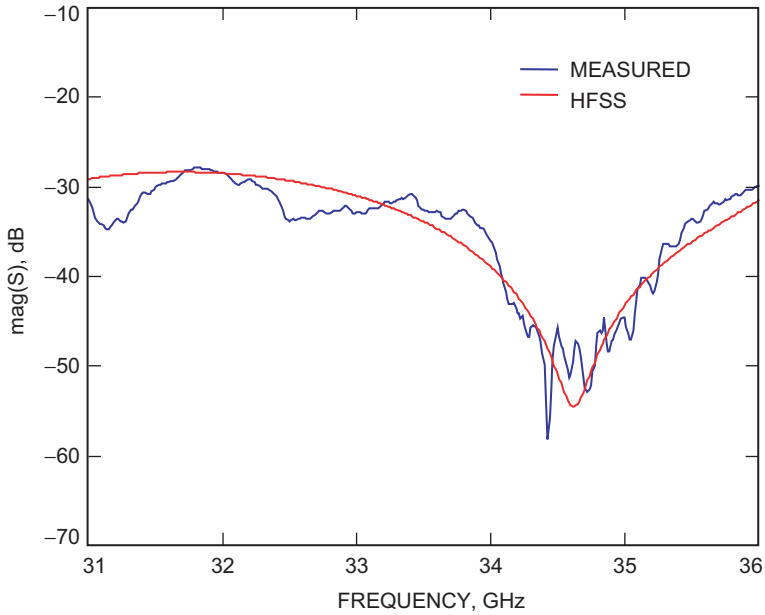

Fig. 10. Radial base input match for equal excitation of all input ports when terminated with a circular waveguide matched load.

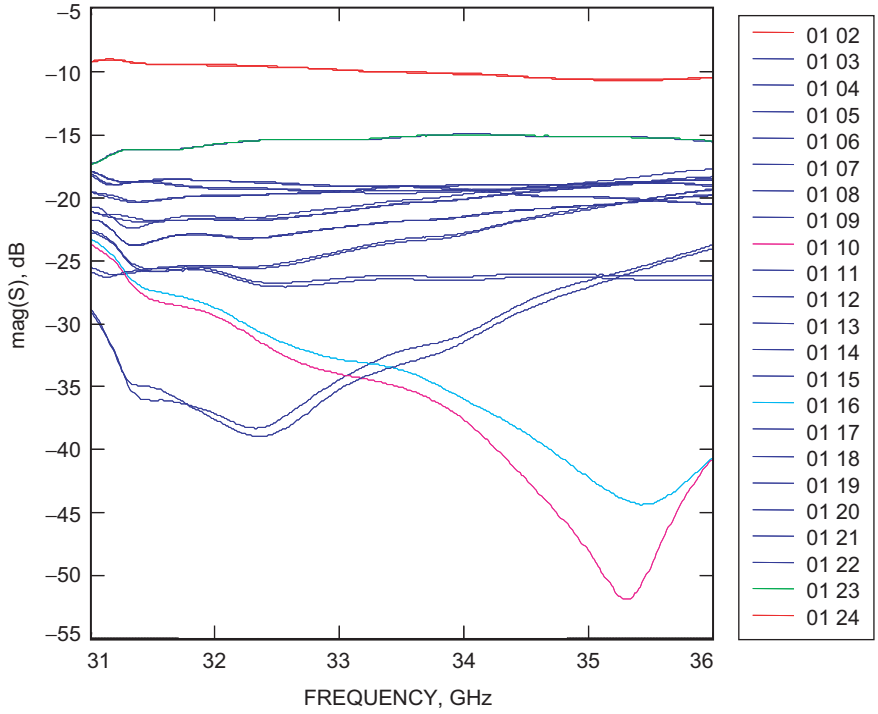

Fig. 11. Isolation between rectangular input ports, mag (S_{21}), of the radial base when terminated with a circular waveguide matched load.

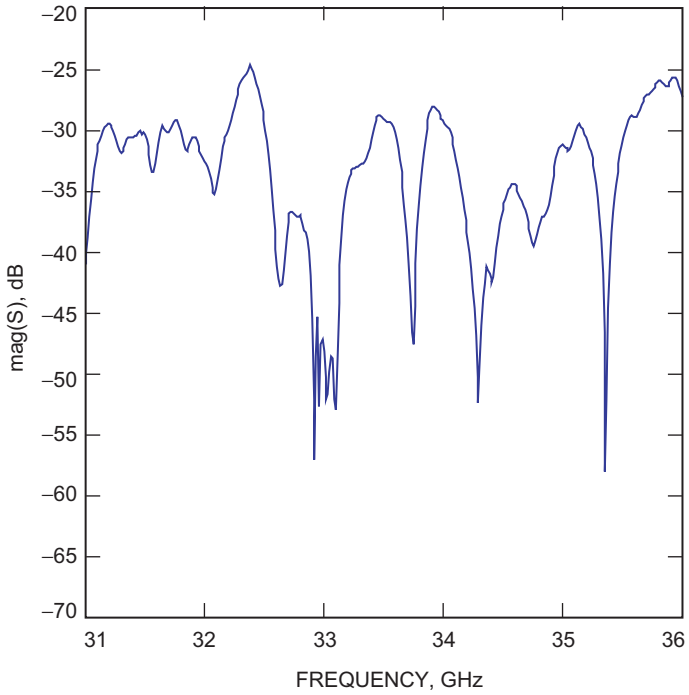

Fig. 12. Radial combiner output match with all input ports terminated. The symmetry plane of the Marie-mode transducer was aligned between RWG ports in the radial base.

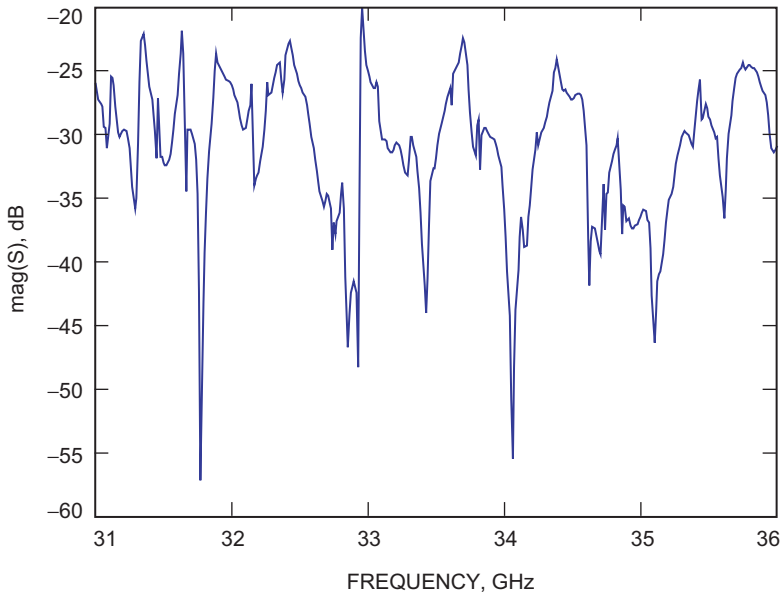

Fig. 13. The 24-way radial combiner input match for equal excitation of all input ports. The symmetry plane of the Marie-mode transducer was aligned between RWG ports in the radial base.

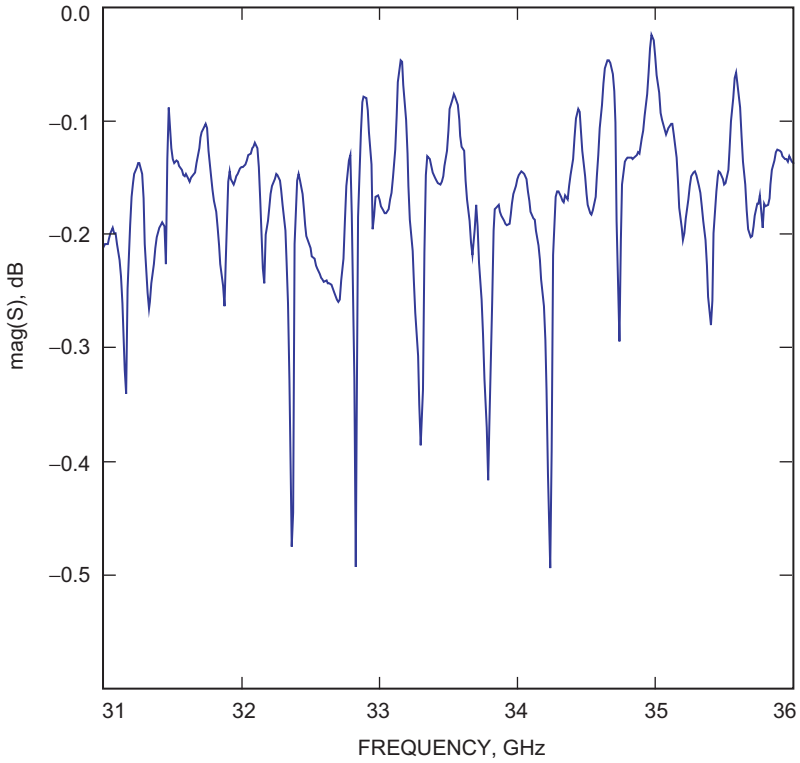

Fig. 14. 24-way waveguide radial combiner insertion loss. Total S_{21}/insertion loss (corresponding to combining efficiency) computed by adding the coupling of 12 ports and using symmetry: the symmetry plane is aligned between RWG ports in the base.

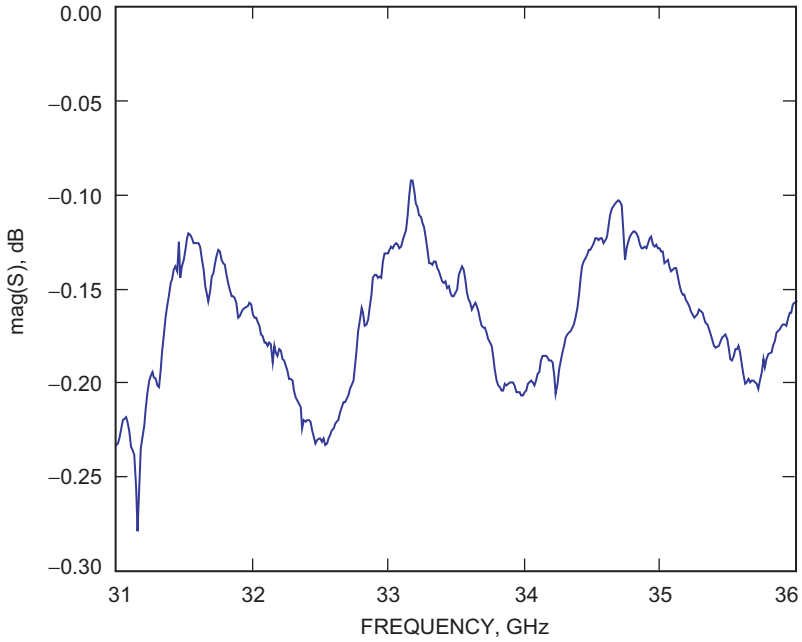

Fig. 15. 24-way waveguide radial combiner insertion loss. Total S_{21} insertion loss (corresponding to combining efficiency) computed by adding the coupling of 24 ports: the symmetry plane is aligned between RWG ports in the base.

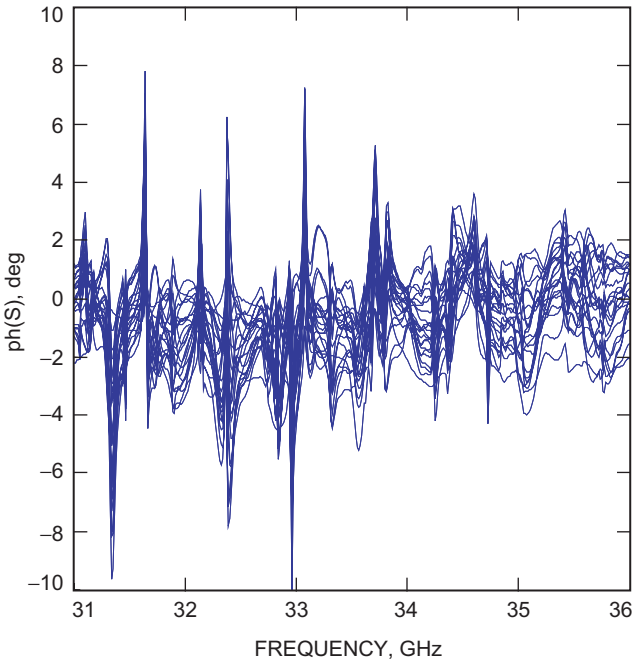

Fig. 16. Insertion phase at the output port of the 24-way radial combiner from the different input ports. Data are normalized to the insertion phase from input port 1 to the output port.

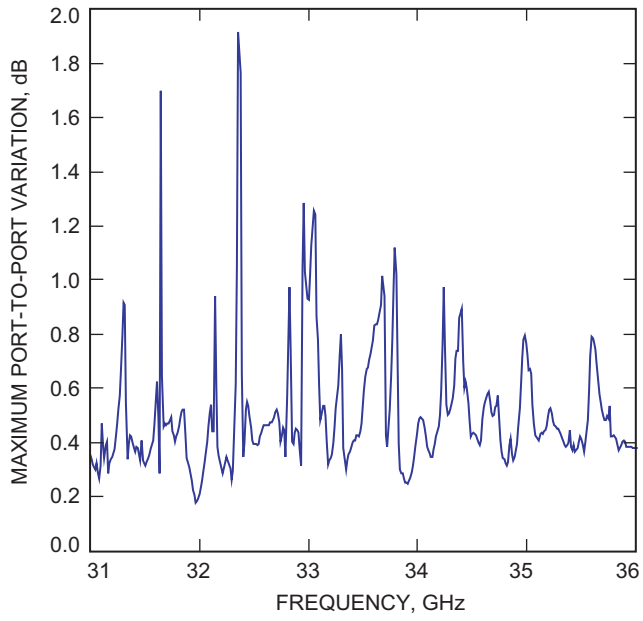

Fig. 17. Maximum amplitude variation among the 24 input ports of the radial combiner as a function of frequency. The combiner was fed from the output port, i.e., the mode transducer, with the symmetry plane aligned between RWG ports in the base.

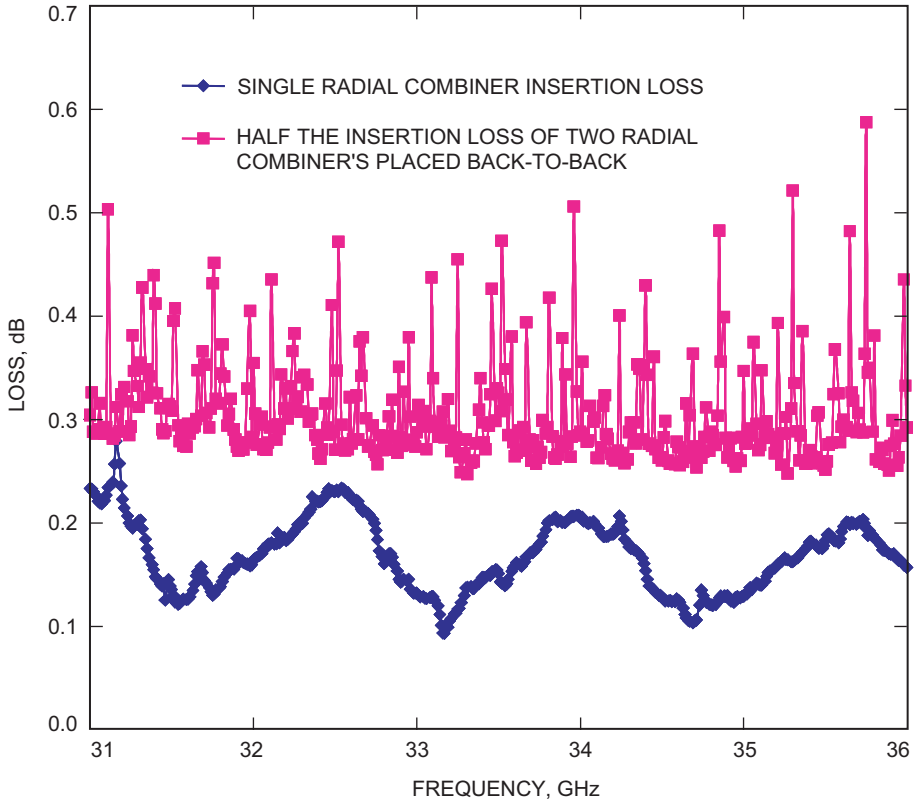

Fig. 18. Comparison of insertion loss of two back-to-back 24-way radial combiners to that of a single radial combiner.

Fig. 13 from the measured data, an assumption that would result in the use of only 12 ports. Figure 13 was computed for the alignment of the mode transducer between two RWG ports in the base (ports 24 and 1).

Figure 14 shows the overall insertion loss, which corresponds to combining efficiency, computed by adding the coupling measurements from 12 ports and using a symmetry assumption. As a comparison, on removing the assumption of symmetry and using 24 input ports instead of 12 input ports, the remaining 12 measurements were completed, resulting in Fig. 15. The measurements in Fig. 15 show a reduction in the ripple behavior caused by asymmetry in the combiner's parts (removal of the symmetry assumption) from roughly ∼0.3 dB to ∼0.1 dB peak-to-peak. This change may be indicative of trapped-mode effects, which can be caused by part asymmetry, especially in the transducer. Trapped modes can exist between the transducer and radial combiner in the over-moded circular waveguide section.

A more clear indication of trapped-mode effects is shown in the insertion phase variation at the output port as it relates to the different input ports (Fig. 16). The phase is normalized to one of the input ports. The associated amplitude variation is shown in Fig. 17.

Figure 17 shows frequencies where the amplitude balance degrades away from an equal 1/24th split. For the combiner to have the minimum insertion loss, it would be required for the monolithic microwave integrated circuit (MMIC) amplifier modules to feed it on a port-to-port basis, consistent with Figs. 16 and 17. This would require variation over the frequency band. What is the additional loss if the MMIC amplifiers were not to feed the power combine as required? That is, what is the effect of the amplitude and phase imbalances of Figs. 16 and 17?

At the conclusion of this task, we had only begun to look at the theoretical calculation of input amplitude and phase imbalance on the output of the 24-way radial combiner. As a quick measurement to determine the effect, two radial combiners were placed back-to-back. Any imbalance at the output of the first radial divider (combiner) then is reflected in the input of the radial combiner. In fact, the phases from the input radial divider result in a doubling of phase error feeding the radial combiner, away from the desired conjugate phase matching.

Figure 18 compares the insertion loss of the two radial combiners in a back-to-back configuration to a single combiner. The offset in loss of the comparisons reflects the copper loss of 11.43 cm (4.5 in.) of WR-28 copper waveguide H-bends, amounting to ∼0.07 dB, plus the additional loss from the amplitude and phase imbalance. One could conclude from the loss of the back-to-back test that the additional insertion loss from amplitude and phase imbalance is ∼0.4 dB minus the estimated waveguide loss of 0.07 dB, or ∼0.33 dB over the band. This 0.33 dB then reflects the amplitude imbalance as shown in Fig. 17, and double the phase imbalance of Fig. 16.

In conclusion, this combiner has an input match <-20 dB under equal excitation of all input ports, an output match <-24 dB at the RWG port of the Marie transducer, and an insertion loss <0.3 dB. The functional bandwidth of the combiner exceeds the initial design band of 31 to 36 GHz. Some effects indicative of trapped modes have been found in measurements, with some initial investigation to determine their effects on the combining efficiency. Some additional investigation is needed in order to calculate the theoretical effects of amplitude and phase imbalances on the 24-way radial combiner's combining efficiency, and to study the mode filters that are used to reduce these effects.

C. Transmission Line Loss Validation

In the first article [1], mass estimates were made for prototype systems. In order to keep mass to a minimum, it is desirable to use aluminum instead of copper. One obvious disadvantage of aluminum is its lower conductivity as compared to other conductors; see Table 1.

JPL typically plates both aluminum and copper parts intended for space applications with gold to form a passivation layer. This protects materials such as aluminum, which readily form an oxide layer.

In order to get the weight savings of aluminum without its associated increased waveguide loss, a quick hardware validation exercise was undertaken to investigate the possibility of plating aluminum WR-28 waveguide with silver, and to determine the effect of additional polishing after machining. As baseline comparisons, gold plating and aluminum waveguide also were tested.

The WR-28 aluminum waveguide test piece is machined from aluminum 6061-T6, with a length of 1 ft (30.48 cm); see Fig. 19. The test articles were plated as follows:

(1) 2.54 μm (100 μin.) Ag to ASTM-B-700 Type-1, Grade A, Class N, using Epner Technology's proprietary High Q^{TM} Silver process[4]

(2) 2.54 μm (100 μin.) Ag as above, but prior to coating, polish to 0.41 μm (16 μin.) finishes on the three surfaces indicated

(3) 2.54 μm (100 μin.) Au to ASTM-B-488 Type-1

(4) WR-28 waveguide: bare aluminum as machined

The results for these plating types are discussed in the next section.

[4] The High Q^{TM} silver plating process was done by Epner Technology Inc., Brooklyn, New York.

Table 1. Conductivity and skin depth of various conductors at 32 GHz.

Conductor	Conductivity, S/m	Skin depth, μm	Skin depth, μin.
Aluminum (Al)	3.817×10^7	0.45	17.91
Gold (Au)	4.098×10^7	0.44	17.28
Copper (Cu)	5.800×10^7	0.36	14.31
Silver (Ag)	6.173×10^7	0.35	13.95

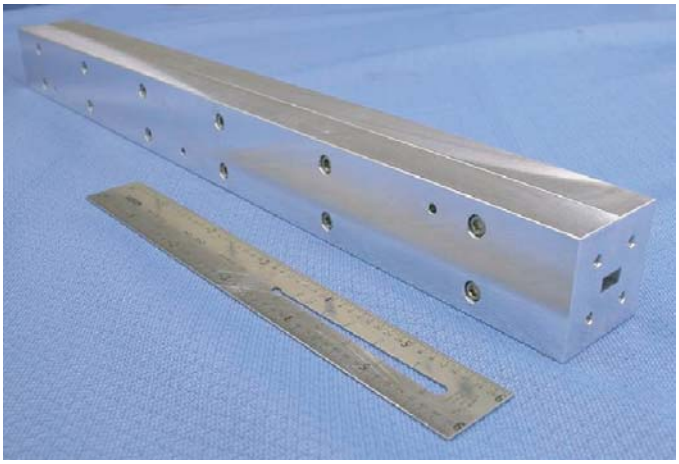

Fig. 19. Aluminum WR-28 straight section, within which the waveguide walls were plated.

1. Rectangular Waveguide Loss Versus Plating. The measured results for the required frequency band of this task are shown in Fig. 20. The results in Fig. 20 indicate there is considerable improvement in plating the aluminum with gold, with additional improvement as expected from the silver plating.

There is, however, not as marked an improvement gained from polishing the machined part prior to plating, which improves the loss to 0.61 dB/m from 0.66 dB/m at 31 GHz. The results of Fig. 20 in measured loss numbers are shown in Table 2. The gold plating decreases the loss (at 31 GHz) of the machined aluminum by ∼0.2 dB/m, while the silver plating decreases the loss in comparison to aluminum by ∼0.3 dB/m. If one assumes that the aluminum is passivated with gold, the silver plating improves over the gold plating by ∼0.1 dB/m. This may be a significant contribution in situations where system waveguide lengths cannot be minimized.

An Ansoft HFSS calculation also is plotted in Fig. 20. This was useful for verifying loss calculations as computed by this design tool, commonly used in calculating the losses of the other system designs discussed in this article. System loss is an important factor in combiner efficiency. It was found that the Ansoft HFSS calculation using a gold conductivity of 3.3×10^7 S/m more closely matched that of the measurements than the theoretical value of pure gold, 4.1×10^7 S/m.

2. Aluminum, TE_{01}, Circular Waveguide Loss Based on Mode Transducer Measurements. As a final data point, this task was able to measure the TE_{01} circular waveguide mode loss using the mode transducers of Fig. 6. The TE_{01} circular waveguide mode is considered a low-loss propagation mode. Consider two of the mode transducers measuring a length of aluminum circular waveguide, where the length is 12.2 cm (4.805 in.). In order to perform this measurement, a through-reflect-line (TRL)

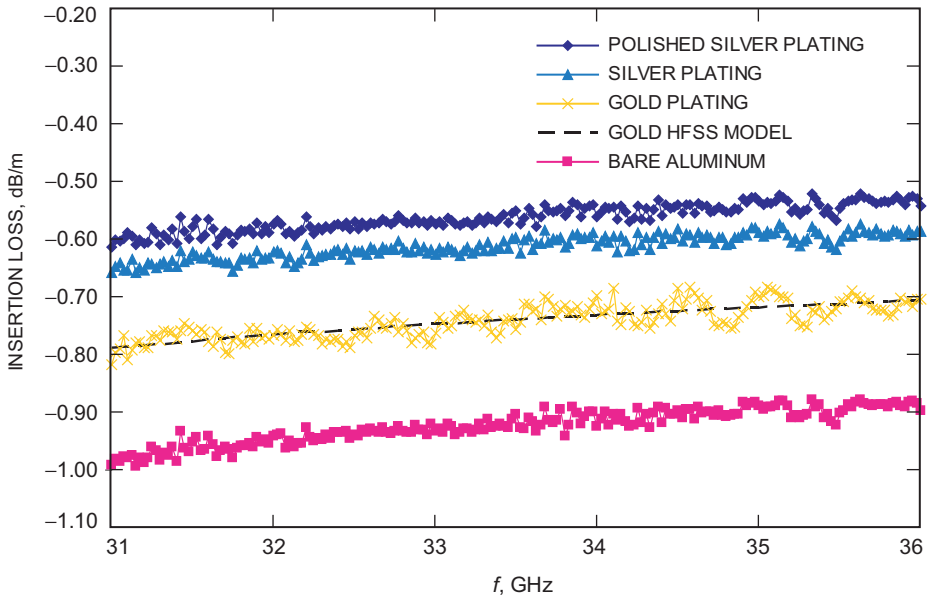

Fig. 20. Insertion loss of the plated aluminum WR-28 straight section.

Table 2. Aluminum WR-28 straight section, within which the waveguide walls were plated.

Plating metal	Loss, dB/m	
	31 GHz	36 GHz
Silver-polished	0.61	0.54
Silver	0.66	0.59
Gold	0.79	0.71
Aluminum	0.99	0.90

calibration was done to the circular waveguide flange of the mode transducers using a 0.513-cm (0.202-in.) section of aluminum guide as the "line" in the calibration. We note that such a calibration is valid only in the case of single-mode propagation at the circular waveguide port of the mode transducers, which the built mode transducers only approximate to the extent they produce only the TE_{01} CWG mode. This approximate measurement of the S_{21} of a circular waveguide section of 1.64-cm (0.65-in.) diameter is shown in Fig. 21. The range of measurements extends down to 28 GHz.

To smooth out the effects of the limitations of the calibration, a 10-point moving average computation of the insertion loss is shown in Fig. 22. From this measurement, the insertion loss of the TE_{01} circular mode in aluminum is approximately 0.3 dB/m at 31 GHz and 0.25 dB/m at 36 GHz (ignoring the spike due to measurement calibration error). The circular aluminum waveguide loss is 0.65 dB/m less than the silver-plated WR-28 rectangular waveguide. This helps explain the low loss measured in the Marie-mode transducer built, given the length of the transducer.

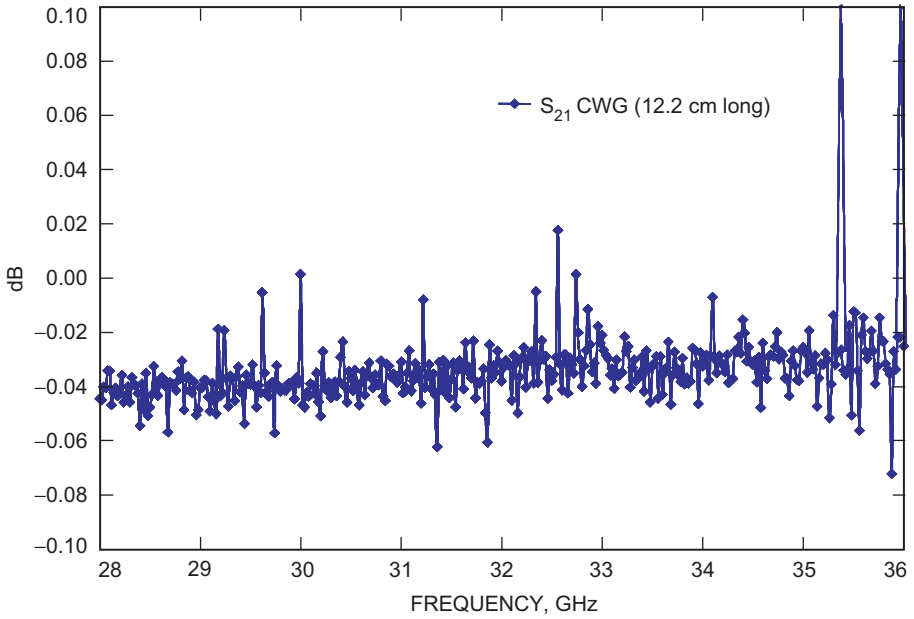

Fig. 21. S_{21} of circular aluminum waveguide measured between two Marie-mode transducers.

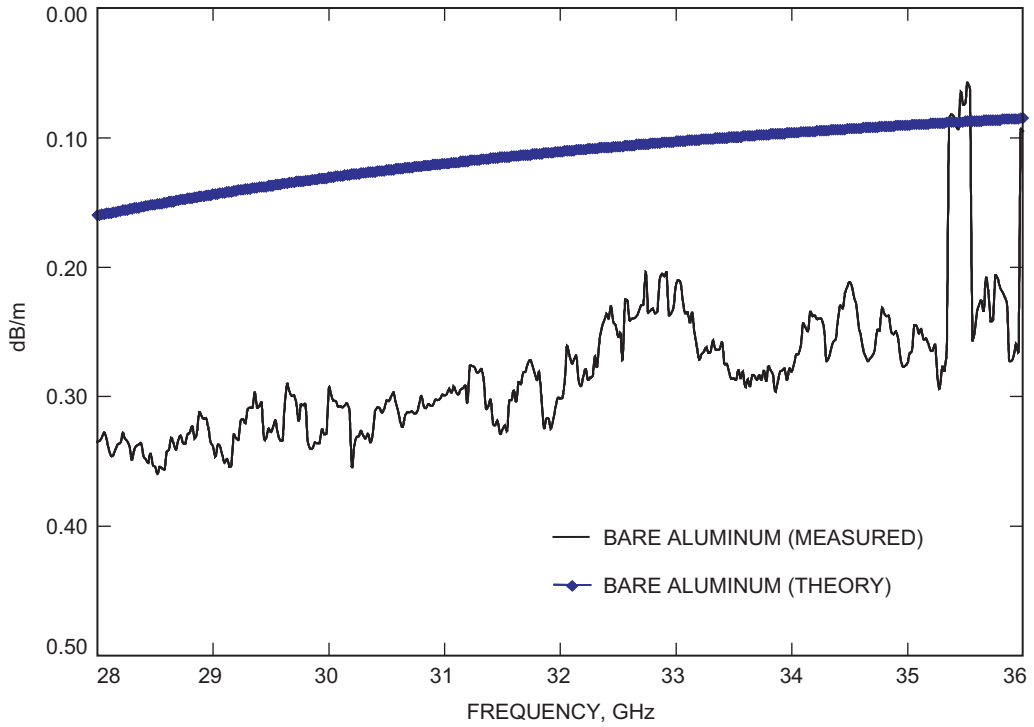

Fig. 22. CWG TE_{01} insertion loss of aluminum waveguide measured between two Marie-mode transducers using a 10 frequency moving average, compared to theory (3.72×10^7 S/m).

III. SSPA Architecture Comparison

A. RF Performance of Power Combiners

The RF performance of the three power combiners evaluated in this study, a 16-way septum combiner, a 24-way waveguide radial combiner, and a 32-way parallel-plate radial combiner, are summarized in Table 3. Each combiner represents a point design, and each can be scaled to alternate numbers of combining ports if required.

As can be seen in Table 3, although the number of combining ports varies by a factor of two, the combining efficiencies are nearly identical for the three power combiners. The initial target of total combining loss <1 dB seems achievable by each combiner for its respective number of combining ports.

Although the bandwidth of all three combiners exceeds the requirement, the radial combiner offers greater bandwidth compared to the other combiners. The bandwidth of the Marie transducer, a key component of the waveguide radial combiner, is determined by its length. In future designs, it may be possible to reduce the length of the transducer and thereby trade some excess bandwidth for reduced mass and volume.

B. Required MMIC for Each Combiner

The required MMIC for each combiner type is listed in Table 4. To achieve a 40 percent power-added efficiency (PAE) SSPA, the required MMIC PAE is >48 percent. To achieve 120-W SSPA output power, the required MMIC power is 9.1 W, 6.0 W, and 4.5 W, respectively, for 16, 24, and 32 MMICs combined.

Table 3. RF performance of power combiners evaluated in this study over the 31- to 36-GHz band.

Power combining	No. of ports combined N	Input match, dB	Output match, dB	Isolation, dB	Total combining loss,[a] dB	Combining efficiency, percent	Source
Septum	16	25	31	27	0.87	82	Analysis
Waveguide radial	24	20	25	7	0.80	83	Measured
Parallel plate	32	24	22	20	0.80	83	Analysis

[a] This includes an estimated 0.45-dB loss for the MMIC package and transition. It also includes a 15 percent margin.

Table 4. Required MMIC performance for 120-W, 40 percent PAE SSPA.

Power combiner	No. of MMICs combined N	MMIC power, W	MMIC PAE, percent
Septum	16	9.1	49
Waveguide radial	24	6.0	48
Parallel plate	32	4.5	48

If larger MMICs are successfully developed, re-design options for power combiners with an alternate number of combining ports are as follows. Given the binary architecture of the septum combiner, an 8-way version can be easily implemented. An 8-way combiner, however, would require at least an 18-W MMIC. For MMIC powers between 9 W and 18 W, the binary architecture cannot be used since the number of combined ports must be a power of 2. The radial combiners, however, do not have this constraint. It should be possible to implement any number of combining ports between 8 and 24 to match the available MMIC power. A 12-way radial combiner (waveguide or parallel-plate) design, for example, would require a 12-W MMIC.

For all three combiner types, the combining loss is a weak function of the number of combining ports. Thus, regardless of the MMIC output power, the required MMIC efficiency will remain relatively constant at ∼50 percent.

C. Combiner Mass and Volume Estimates

The prototype dimension and mass estimates are listed in Table 5. The prototype designs include significant additional mass that is expected to be eliminated in flight implementations.

The mass and volume of an SSPA based on the septum combiner scales in a binary fashion. An 8-way septum combiner, for example, would have approximately half the mass and volume compared to a 16-way combiner. The size of a septum combiner SSPA is limited by the layout of the combiner waveguide runs. Reducing the dimensions of the MMIC module (Fig. 1 of [3]), for example, would have little effect on the SSPA mass and volume. Any reduction of mass would be due to trimming excess metal only.

In contrast, the radius of a radial combiner is determined primarily by the width of the MMIC module. Assuming thermal considerations would allow the MMIC modules to be placed adjacent to each other, we can relate the circumference of the combiner, C, to the MMIC module width, w, and the number of ports, N, as follows:

$$C = 2\pi \cdot r \approx N \cdot w$$

Since volume and mass are proportional to the square of the radius, the volume and mass of a radial combiner scale approximately proportional to $(Nw)^2$. The prototype radial combiners were designed to accommodate MMIC modules with standard WR-28 flanges. If custom flanges are implemented, the width of the module can be reduced by ∼30 percent. This suggests the mass of the waveguide radial base and the parallel-plate combiner can be reduced to ∼50 percent of the mass listed in Table 5.

D. Advantages and Disadvantages of Each Combiner

Key advantages and disadvantages of the three SSPA architectures are listed in Table 6.

Table 5. Prototype SSPA mass and volume estimates.

Power combiner	No. of ports combined N	Prototype mass,[a] kg	Prototype dimensions, cm	Baseplate area, cm^2
Septum	16	3.7	$23 \times 17 \times 4$	391
Waveguide radial	24	4.4	$28 \times 28 \times 66$	615
Parallel plate	32	4.6	$32 \times 32 \times 4$	804

[a] Excludes electronic power conditioner (EPC). Flight mass will be reduced by milling excess metal.

Table 6. Advantages and disadvantages of SSPA architectures.

Power combiner	Advantages	Disadvantages
Septum	·Simple form factor ·Binary architecture easily scalable ·Single-mode structure	·Precision machining ·Assembly of resistive cards
Wavequide radial	·Very high power handling capability ·Very wide bandwidth	·Complex fabrication ·Dimensions less compact ·Over-moded structure may introduce amplitude ripple (which translates to phase ripple) over bandwidth
Parallel plate	·Simple machining and assembly ·Highly scalable in both frequency and number of ports	·Power handling limited by breakdown at central coaxial probe ·Over-moded structure ·Lowest technology readiness level: design complete, but no proof-of-concept hardware to date

IV. Conclusions and Recommendations for Continuing Investigation

A. The MMIC Package and Waveguide Transition

The MMIC package and waveguide transition loss (0.45 dB) represents >50 percent of the total combining loss. Therefore, it is easy to point out this area as one of importance, and as an area where development should proceed regardless of the architecture chosen in order to minimize development time. JPL has looked at packaged gallium arsenide (GaAs) components, as shown in Fig. 3. This standard package size, along with the microstrip-to-waveguide transition design of Fig. 5, is incorporated into the proposed MMIC amplifier module with the standard waveguide input and output shown in Fig. 1 of [3]. With the need to reduce microstrip losses by transitioning into waveguide quickly, one could view Fig. 1 of [3] as a baseline design for developing the gallium nitride (GaN) MMIC, package, waveguide transition, and amplifier module.

Initial development could begin using commercial packaging, with prototypes developed for early stage GaN MMICs at lower power levels. As the power levels of the GaN MMICs increase, specifically for the needs of power combiner architectures such as the septum combiner, custom packages would become important for not only an RF design aimed at reducing loss but also from the viewpoint of optimizing the thermal design. Thermal issues at the MMIC package level will directly translate into thermal requirements at the SSPA level. As detailed in [2], any custom package design, and even MMIC outputs, should be biased towards the lower loss of microstrip versus coplanar waveguide (CPW) in both the MMIC and any matching circuitry used between the MMIC and waveguide transition.

B. Suggested Areas of Continuing Investigation

The 24-way waveguide radial power combiner measurements indicated some trapped-mode effects, which typically are suppressed by adding mode filters. However, time did not permit investigation and/or testing of mode filters to reduce amplitude and phase effects caused by trapped modes. For example, a next logical step would be the design and fabrication of circular waveguide transitions to adapt to commercial helical filters, combined with an investigation of other types of mode filters. Also, high-power testing of back-to-back radial power combiners should be done, to the extent possible, with existing high-power sources.

The septum combiner should be high-power tested for characterizing thermal performance limits and RF performance at the required power levels of the proposed system. This would be followed by design iteration for improving manufacturability and thermal robustness, if required, based on test results.

A prototype 32-way parallel-plate combiner should be fabricated to validate the RF design [12].[5] This architecture had the lowest technology readiness level at the time of the hardware build. That should not necessarily exclude this design from consideration. A proof-of-concept hardware demonstration of this architecture would place it in a position to be more equally compared to the hardware presented in this article.

Acknowledgments

The authors would like to acknowledge the following individuals for making significant contributions to the work documented in this article: Daniel J. Hoppe, JPL, and Dan Kelley, Honeywell Technology Solutions, Inc.

References

[1] P. Khan, L. Epp, and A. Silva, "Ka-Band Wide-Bandgap Solid-State Power Amplifier: Architecture Identification," *The Interplanetary Network Progress Report*, vol. 42-162, Jet Propulsion Laboratory, Pasadena, California, pp. 1–16, August 15, 2005. http://ipnpr.jpl.nasa.gov/progress_report/42-162/162E.pdf

[2] P. Khan, L. Epp, and A. Silva, "Ka-Band Wide-Bandgap Solid-State Power Amplifier: General Architecture Considerations," *The Interplanetary Network Progress Report*, vol. 42-162, Jet Propulsion Laboratory, Pasadena, California, pp. 1–19, August 15, 2005.
http://ipnpr.jpl.nasa.gov/progress_report/42-162/162F.pdf

[3] P. Khan, L. Epp, and A. Silva, "A Ka-Band Wide-Bandgap Solid-State Power Amplifier: Architecture Performance Estimates," *The Interplanetary Network Progress Report*, Jet Propulsion Laboratory, Pasadena, California, vol. 42-163, pp. 1–17, November 15, 2005.
http://ipnpr.jpl.nasa.gov/progress_report/42-163/163A.pdf

[4] A. R. Khan, L. W. Epp, D. J. Hoppe, and D. Kelley, *Thin-Film Resistive Septum Waveguide Power Combiner*, provisional patent application no. 48,467, docket number CIT-4300-P, filed January 21, 2005.

[5] L. W. Epp, D. J. Hoppe, A. R. Khan, and D. T. Kelley, *Wideband (31 to 36 GHz) 24-Way Radial Power Combiner/Divider Fed by a Marie Transducer*, provisional patent application, CIT File no. CIT-4336-P, filed March 18, 2005.

[5] A. R. Khan, L. W. Epp, and D. J. Hoppe, *Wideband (31 to 36 GHz) Parallel Plate Power Combiner/Divider with Isolation*, JPL New Technology Report no. 41758 (internal document), Jet Propulsion Laboratory, Pasadena, California, January 31, 2005.

[6] H. A. Hoag, S. G. Tantawi, R. Callin, H. Deruyter, Z. D. Farkas, K. Ko, N. Kroll, R. L. Lavine, A. Menegat, and A. E. Vlieks, "Flower-Petal Mode Converter for NLC," *Proceedings of the 1993 Particle Accelerator Conference*, vol. 2, pp. 1121–1123, May 17–20, 1993.

[7] "330 Series TE_{01} Mode Transitions Data Sheet," Millimeter Products, Inc. (MPI), http://www.milpi.com/330main.html. MPI is now part of QuinStar Technology, Inc., Torrance, California.

[8] S. S. Saad, J. B. Davies, and O. J. Davies, "Analysis and Design of a Circular TE_{01} Mode Transducer," *Microwave, Optics and Acoustics*, vol. 1, pp. 58–62, January 1977.

[9] P. H. Wolfert, "A Wide-Band Rectangular-to-Circular Mode Transducer for Millimeter Waves (Correspondence)," *IEEE Transactions on Microwave Theory and Techniques*, vol. 11, issue 5, pp. 430–431, September 1963.

[10] M. H. Chen, "A 19-Way Isolated Power Divider via the TE_{01} Circular Waveguide Mode Transition," *IEEE MTT-S International Microwave Symposium Digest*, vol. 86, issue 1, pp. 511–513, June 2, 1986.

[11] *High Frequency Structure Simulator (HFSS)*, 9 ed., Ansoft Corporation, Pittsburgh, Pennsylvania, 2003.

[12] A. R. Khan, L. W. Epp, and D. J. Hoppe, *Wideband (31 to 36 GHz) Parallel Plate Power Combiner/Divider with Isolation*, provisional patent application, CIT File no. CIT-4372-P, filed May 3, 2005.